Light Metals 2013 *Edited by: Barry Sadler*
TMS (The Minerals, Metals & Materials Society), 2013

MATHEMATICAL MODEL VALIDATION OF ALUMINIUM ELECTROLYSIS CELLS AT DUBAL

Abdalla Zarouni[1], Lalit Mishra[1], Marwan Bastaki[1], Amal Al Jasmi[1], Alexander Arkhipov[1], Vinko Potocnik[2]

[1]Dubai Aluminium (DUBAL), PO Box 3627, Dubai, UAE
[2]Vinko Potocnik Consultant Inc., 2197 rue de Régina, Jonquière, Québec, Canada, G7S 3C7

Keywords: Mathematical models, Model validation, Aluminium electrolysis cells, DX technology, DX+ technology

Abstract

In recent years DUBAL has developed an in-depth mathematical modeling capability for aluminium electrolysis cells, based on commercial software packages, comprising thermo-electric, MHD and mechanical models of the cells as well as CFD models of gas extraction from cells and of potroom ventilation. In order to validate these models a measurement program was initiated, consisting of a group of DX and DX+ cells instrumented for continuous monitoring of cathode lining and potshell temperatures, busbar temperatures and busbar currents. Moreover, special measurement campaigns were carried out for cell voltage breakdown, heat fluxes, freeze profiles, current distribution, magnetic fields, metal velocities, potshell deformation and cell gas exhaust flow rate. The modeling results showed excellent agreement with measured data, allowing the models to now be used with confidence for new cell designs and industrial studies of existing potlines. In this paper, detailed measurement and modeling results shall be discussed.

Introduction

Mathematical modeling has become a primary design and optimization tool of aluminium electrolysis cells. In the early years of mathematical modeling, the models were based on in-house software, specifically designed for different processes in the electrolysis cells. These models required large development effort; however, when developed, their usage was low cost. This is why they are still used in some companies, together with newer models based on commercial software packages. The advantage of commercial software packages is that they are being continuously developed and maintained, whereas this is often not so with in-house software. General commercial software packages also had to be adapted for specific processes and geometry of aluminium electrolysis cells and potrooms, which in addition required considerable effort and time, often many man years per model. Most of these models are proprietary, but some are generic and available on the market. This is the case with ANSYS based thermo-electric and mechanical models [1 - 3] and ESTER/PHOENICS (henceforth called ESTER) based MHD models of the cells (ESTER is a specific adaptation of CFD software package PHOENICS for aluminium electrolysis cells) [4 - 6]. On the other hand, there are also specific commercial software packages developed for a specific domain; this is the case of MHD software package MHD-VALDIS that performs all calculations for busbar design, electric current distribution, magnetic fields, steady state MHD and cell stability [7]. A more limited scope software package MARC (Magnetics in Aluminum Reduction Cells) uses specified busbar currents and cell steel to calculate magnetic fields in the cells, in the potrooms or anywhere else in the smelter [8]. Its magnetic field in the cells is then used in ESTER, together with vertical current density at the bottom of metal pad from ANSYS, to model cell MHD.

DUBAL model development started with the concept that full modeling capability can be achieved rapidly if public, generic models, based upon commercial software packages are utilized so that all the processes required for the cell design and optimization are included. These models include automatic data transfer between them if required. The software packages used are: ANSYS, PHOENICS, MHD-VALDIS with TECPLOT graphics [9] and MARC. In some cases the same process is modelled with two software packages in order to validate model results against each other, thus increasing the model reliability. For example, busbar currents and temperatures are calculated with ANSYS and MHD-VALDIS; magnetic fields are calculated with MARC and MHD-VALDIS; MHD is calculated with ESTER and MHD-VALDIS. DUBAL modeling capability comprises thermo-electric models based on ANSYS, busbar design models based on ANSYS and MHD-VALDIS, MHD models based on MHD-VALDIS and a combination of ANSYS - MARC - ESTER, mechanical models based on ANSYS and CFD models of cell gas extraction and potroom ventilation based on PHOENICS.

Modeling is not an exact science that can predict cell parameters from theoretical principles only. Measurements of every calculated measurable parameter are needed in order to validate the models. At DUBAL an extensive measurement program was set up, consisting of a group of DX and DX+ cells instrumented for continuous monitoring of cathode lining and potshell temperatures, busbar temperatures and busbar currents. Moreover, numerous special measurement campaigns have been carried out for cell voltage breakdown, heat fluxes, freeze profiles, current distribution, magnetic fields, metal velocities, potshell deformation and cell gas exhaust flow rate. The measurement techniques are well known and are described elsewhere [10]. In this paper it will be demonstrated how these measurements were used for model validation on DX or DX+ cells.

Electrical Measurements and Model Validation

Electrical measurements comprise cell voltage drops, busbar temperatures and busbar current distribution. Figure 1 shows how cell voltages are decomposed. Cell voltage components consists of the following: anode voltage drop from below the anode clamps to the anode bottom, cathode voltage drop from the metal pad to the end of the collector bars and busbar (or external) voltage drop from the end of the collector bars to below the anode clamps. As per DUBAL practice in DX and DX+ cells, two intermediate reference measurement points on the busbars are used: Cathode Reference Point (CRP) on the downstream cathode busbar just outside the tap end collector bar and Anode Reference Point (ARP) on the anode cross-beam busbar at the duct end of the cell. In practice, the voltage drop between the metal pad and CRP is measured ($V_{cat\text{-}CRP}$), then from CRP to ARP ($V_{CRP\text{-}ARP}$) and then from ARP to below each anode clamp ($V_{ext\text{-}an}$). Next, the

voltage between the end of each collector bar and CRP is measured; this is called "Short Drop" in DUBAL terminology. Finally, cathode voltage drop (V_{cat}) and external voltage drop (V_{ext}) are calculated as per Equation (1):

$$V_{cat} = V_{cat-CRP} - Short\ Drop$$
$$V_{ext} = Short\ Drop + V_{CRP-ARP} + V_{ext-an} \quad (1)$$

In this or any other measurement path with reference points, there must be no gaps and no overlap at the reference points. Back EMF (BEMF) and bubble voltage drop are calculated from known equations [11]. From all these voltage components, bath voltage drop and anode-to-cathode distance (ACD) are calculated, but these are not used in model validation.

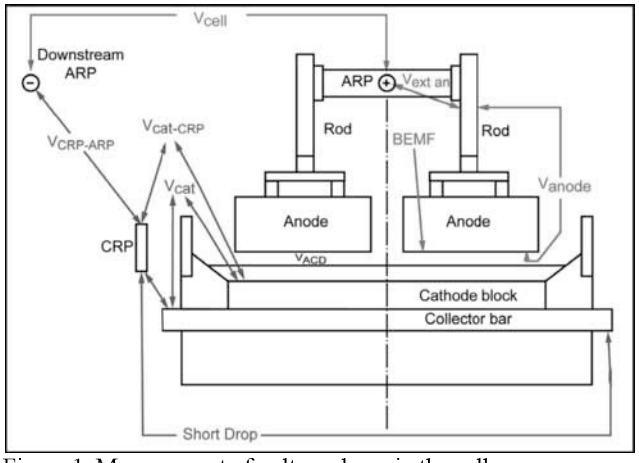

Figure 1. Measurement of voltage drops in the cell.

The cathode and anode model calibrations are made with the carbon block-steel contact resistance chosen so that the overall calculated cathode and anode voltage drops are equal to the measured ones. The busbar voltage drops include two contact resistances: one on the cathode collector bar to flex tabs and the other on the anode beam to anode rods contacts (clamp drop). These were added to ANSYS and MHD-VALDIS model so that the calculated short drop and anode external drop had good visual fit onto the measured values as shown in Figure 2 - 5. Both models agree very well with each other and with measured data.

A further important design parameter obtained from the thermo-electric and busbar modeling was the collector bar current distribution. Collector bar currents were obtained from measured voltage drops across the cathode flexes and flex temperatures. Modeling showed an excellent balance between upstream and downstream currents of 50.5 % upstream and 49.5 % downstream. This compared well with the measured data of 51.3 % upstream and 48.7 % downstream. Figure 6 shows the model current distribution in the upstream and downstream collector bars, compared to the measured data.

Busbar currents and temperatures are monitored continuously in a group of DX and DX+ cells on upstream and downstream cathode busbars that feed the anode risers. Anode riser currents were measured manually. Individual busbar currents and upstream/downstream balance were compared with the models. The difference between models and measurements in individual busbars was smaller than 5 % on the upstream side and smaller than 10 % on the downstream side. The agreement in anode riser currents was within ± 1 %.

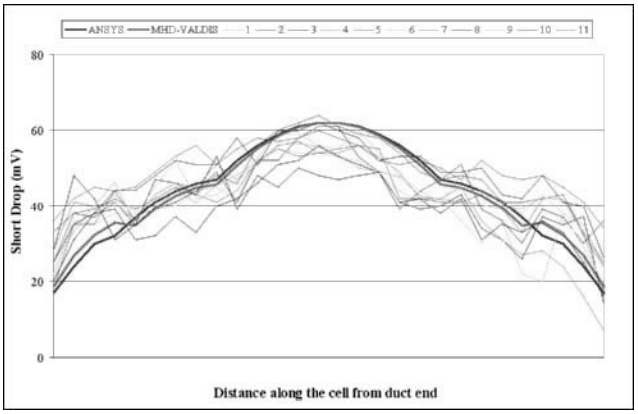

Figure 2. Model validation with measured upstream (US) Short Drops in cells at 420 kA. Numbers on curves indicate individual measurements.

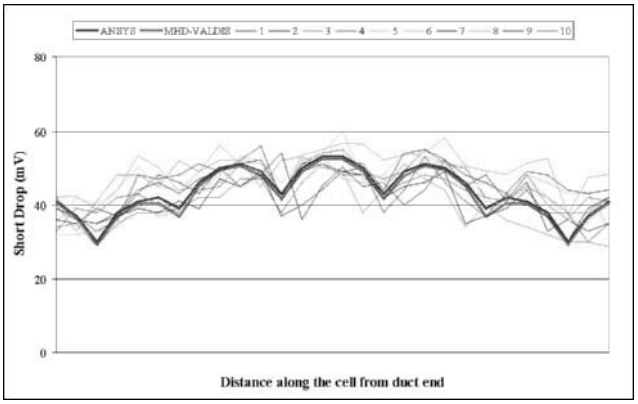

Figure 3. Model validation with measured downstream (DS) Short Drops in cells at 420 kA. Numbers on curves indicate individual measurements.

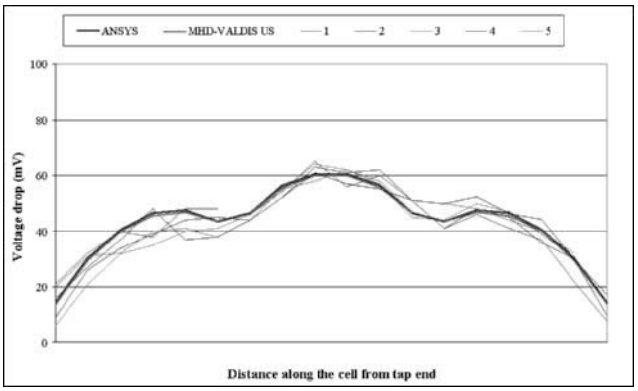

Figure 4. Model validation with measured upstream (US) anode external voltage drops in cells at 420 kA.

Upstream to downstream current balance was within less than ± 1 % in both, the model and the measured data. The difference between the modelled and measured busbar temperatures was 0 – 10 °C in downstream busbars and 1 – 15 °C in upstream busbars. The largest difference was in the busbars close to the potshell and in the outside anode risers. It became evident that the problem was that only one ambient temperature was used in the models for all the busbars, whereas in practice the ambient air has quite different temperatures around the cells. For example, busbars adjacent to

the cathode potshell receive more heat from the potshell, but the outside anode risers are exposed to a lower ambient temperature than the inside risers. Nevertheless, the agreement between the models and measurements is quite acceptable. Temperature differences between the model and the measurement are the cause of the observed busbar current deviations.

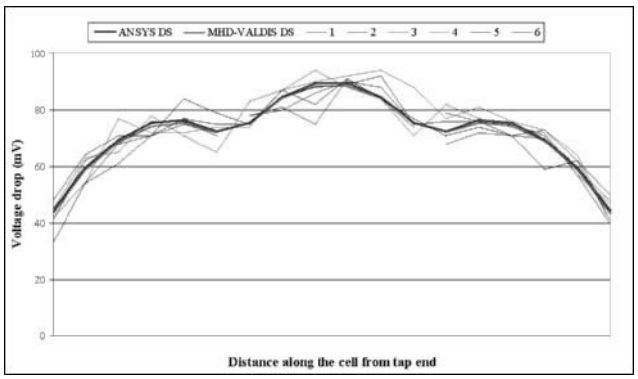

Figure 5. Model validation with measured downstream (DS) anode external voltage drops in cells at 420 kA. Numbers on curves indicate individual measurements.

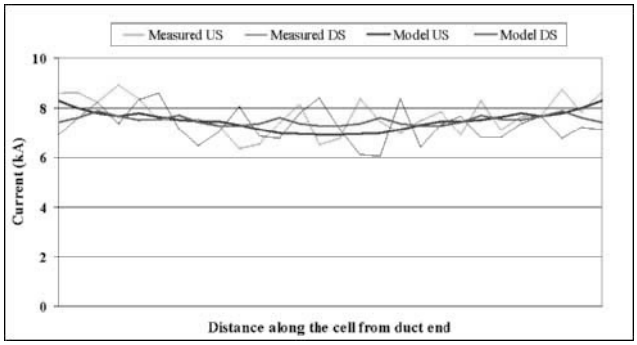

Figure 6. Busbar model validation with measured collector bar currents in cells at 420 kA.

Thermal Measurements and Model Validation

Thermo-electric models provide temperature distribution in the cells and heat loss from the cell. A group of DX and DX+ cells is instrumented with thermocouples on the potshell surface and in the potlining, which monitor the temperatures continuously. These temperatures were used for model validation. Additionally, several measurement campaigns were carried out for more detailed analysis. In these campaigns, voltage components were measured for internal heat calculation, heat fluxes from pre-defined surfaces and additional temperatures on the heat balance surfaces as well as freeze profiles. Heat fluxes were measured with purchased heat flux probes. The temperatures were measured with heat flux probes, infrared pyrometer (IR gun) and by contact surface thermocouples. Figure 7 compares the calculated and measured temperatures on the side surface of the potshell, near the middle of the cells. Measured values have an estimated error bar of ± 30 °C, which is the result of instrument accuracy and standard deviation between the slices. The three measurement methods agree well, but heat flux probes give in general lower temperatures than the other two methods, particularly at high temperatures, because, being inside the heat flux sensor, they are actually at a small distance away from the surface.

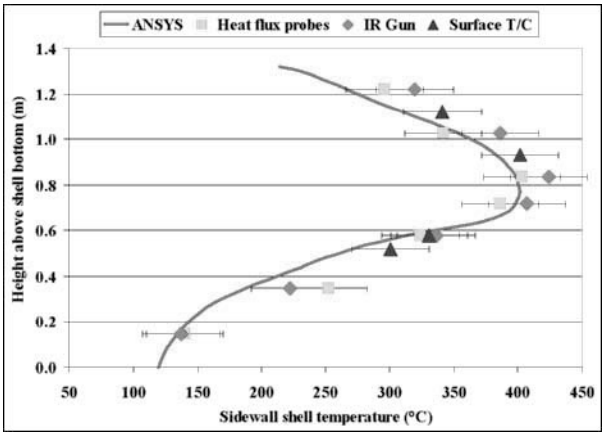

Figure 7. Average side potshell temperature profile near cell centre of three DUBAL cells: ANSYS model compared to measurements with heat flux probes, infrared pyrometer (IR Gun) and contact surface thermocouples (Surface T/C).

For the measurement of cell heat balance, the slice concept is used. This is a measurement strategy applied to a narrow cross-section of the cell, which represents its state at the time of measurement. It has been proven that a limited number of measurement locations on a slice and a limited number of slices on the cell sides and ends can be generalized to the whole surface area of the cell heat balance boundary. The number of measurement points necessary depends on expected variations of heat flux along a slice. As for the cell heat balance boundary, it is common to use one of the two boundaries delimited by System Boundary 1 (over the hood and superstructure) or 2 (see Figure 10). At DUBAL the System Boundary 2 is used for heat balance and System Boundary 1 as the boundary condition for heat loss and temperature for potroom ventilation modeling.

For heat flux measurements, a set of 12 heat flux probes connected to a multichannel data logger was used, supplied by Hukseflux [12]. These were placed along the height of the potshell and on the cradles of three upstream, three downstream slices and of two slices at each end. The same side slices were used over the top of the deckplate and anode cover, including anode rods up to beneath the clamps. From these heat fluxes, the heat loss was calculated from each area represented by a heat flux probe location. The heat balance surface cuts through the anode rods and through the end of the collector bars. Axial heat loss through these cross-sections was evaluated by measuring the temperature gradient along these elements. The overall heat loss was obtained as:

$$Q = \sum_i q_i A_i = \sum_i Q_i \qquad (2)$$

Where: Q = overall heat loss (kW), q_i = heat flux at location i (kW/m²), A_i = area assigned to the location i (m²), Q_i = local heat loss at location i (kW) (the word "heat" is used for power and should be interpreted as heat per second, kJ/s = kW).

Particular attention was given to anode heat loss measurements and modeling. The anode cover thickness was measured on each anode, including an estimation of hard and loose cover thickness. The crust composition was determined in the laboratory and the thermal conductivity was obtained from [13], with some further adjustment of crust composition and crust hardening temperature if needed for good fit to measured heat flux.

Heat flux measurements are prone to errors because of possible problems with heat flux probe calibration and because of great variability of local heat fluxes, particularly on the anode cover. A necessary step in the measurement is to compare the measured heat loss (Q) with the internal heat (Q_{int}), which is the net heat generated inside the heat balance volume, Equation (3):

$$Q_{\text{int}} = (V_{cell} - V_{ext} - V_{Al} + xV_{C\,burn} + yV_{CO\,burn})I \quad (3)$$

Where: V_{cell} = Cell voltage, V_{ext} = External voltage drop as per Equation (1), V_{Al} = Voltage equivalent of enthalpy to make aluminium, $xV_{C\,burn}$ = Fraction x of voltage equivalent of enthalpy of excess carbon burn (air and CO_2), $yV_{CO\,burn}$ = Fraction y of voltage equivalent of CO burn within the chosen heat loss boundary, I = Cell current. V_{Al} includes base electrochemical reactions to make aluminium and all auxiliary processes such as anode butt removal, cavity cleaning, net bath tapping, fluoride feeding, reactions with alumina impurities, etc. All included with no carbon and CO combustion, V_{Al} = 2.09 V for DX+ cells. This value is 2.05 V if 13 % of excess carbon consumption and 10 % CO is assumed to burn and release heat below the crust; this is the same value as for main and back reactions alone, used commonly in the industry. In practice, it is not well known how much excess carbon and CO burn within the System Boundary 2; this remains to be the main uncertainty for the internal energy calculations. However, even with this uncertainty, the internal heat is more accurately known than the one from measured heat flux. In principle, in an exact world, the heat loss is equal to internal heat. It is therefore best to normalise Q to Q_{int} and then multiply all heat fluxes and partial heat losses by the normalisation factor $F = Q_{int}/Q$. This was carried out in this work. Figure 8 shows such normalised measured heat flux from the potshell sidewall in comparison with the ANSYS model, which was run with the cubic spline fit to the measured freeze profile, shown in Figure 9. As expected the highest potshell temperature and heat flux are in the lower half of the metal pad. Figure 10 shows model validation with the overall heat balance, normalised to the same internal heat for both the model and the measurements. The largest difference between the model and measurements is on the cathode side wall, where the model heat loss is greater than the measured one. This could be due to somewhat thinner freeze in ANSYS than the measured one as shown in Figure 9. Overall, it can be seen that the agreement between model and measurements of potshell temperatures (Figure 7), heat flux (Figure 8) and heat loss (Figure 10) is good and the thermo-electric model is considered to be validated.

The normalisation of heat loss to internal heat described above is very important. It is through this process, during the first measurement campaign that it was discovered the calibration of the brand new heat flux probes was not correct; this was finally also recognised by the supplier who had to re-calibrate the probes, using an alternative method from that initially used.

MHD Model Validation

Magnetohydrodynamic (MHD) modeling includes current density distribution in the metal and bath, magnetic field, metal heave, metal and bath circulation patterns and cell stability analysis. Magnetic field was measured with F. W. Bell tri-axial Hall sensor probe gaussmeter. The measurements were made above the crust along the upstream and downstream anode edge because the probe is not made for immersion into the liquid metal. The model simulation outputs were at the same positions. Figure 11 shows the average longitudinal component of the magnetic field above

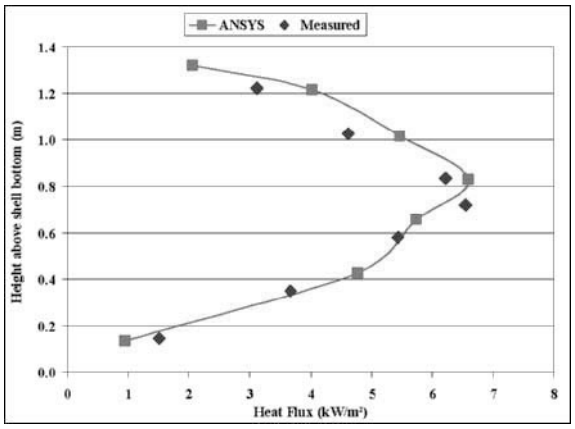

Figure 8. Side potshell heat flux profile near cell centre of a cell: ANSYS model compared to measurements with heat flux probes.

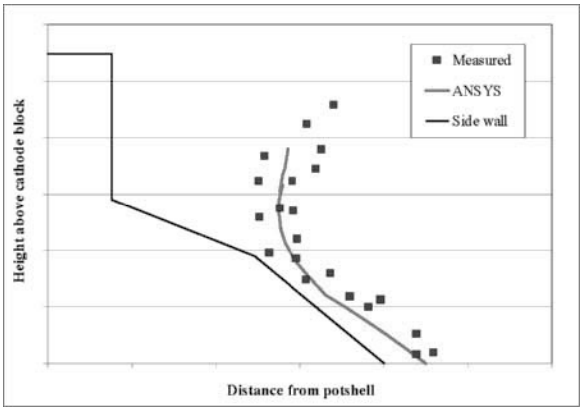

Figure 9. Measured and model freeze profiles.

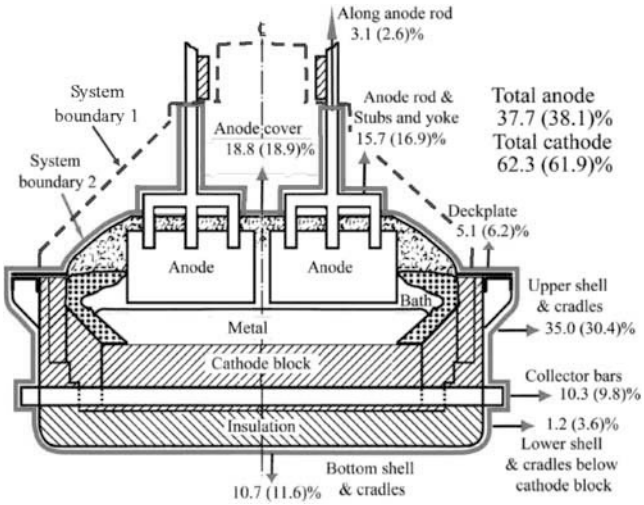

Figure 10. Model validation of overall average heat balance of three cells (the same cells as for Figures 7, 8 and 9) on System boundary 2. The values without brackets are model results, in brackets are measurements.

the crust for three cells. The agreement between the model and the measurements is good except upstream, just behind the anode risers. In this position, the measurement points were very close to the risers and the disagreement is likely due to the lack of detail in the model representation of the riser currents. The metal pad is

further away from the risers than these measurement points and this effect will not be present. It can be concluded that both MARC and MHD-VALDIS are validated for magnetic field calculations in the cells.

Metal velocities were measured with iron rods, using the calibration curves described elsewhere [5, 14]. Special rod holders were designed so that up to six rods could be immersed into the metal pad simultaneously. The measurements were made in the side channels at the corner of each anode, in end channels and in the centre channel near each end. Elsewhere only the centre channel crust-breaker holes were accessible with the iron rods. It was not practical to insert the rods into the narrow gaps between the anodes. Velocity measurements were used to calibrate velocity magnitudes in the models; in ESTER, this was achieved by changing the turbulent viscosity in the model and in MHD-VALDIS by changing the friction coefficient until a good visual fit between the models and measurements was obtained. Figures 12 and 13 show the measured velocities and ESTER model results with calibrated velocity magnitudes. Except for a few locations, very good agreement was observed between the two patterns, both in terms of magnitude and direction. This confirms once again the validity of ESTER velocity calculations.

Metal heaving validation of ESTER and MHD-VALDIS has been proven before and was not repeated during this work [6, 15]. MHD-VALDIS and ESTER gave similar metal heave for DX and DX+ cells.

Mechanical Models

Mechanical models were used to analyze the potshell deformation. The forces responsible for the potshell deformation come from thermal expansion and from the cathode lining expansion due to absorption of chemicals. The thermal expansion is straightforward to model since it uses the temperature distribution obtained from the thermo-electric model and thermo-elastic or thermo-plastic computation is just a further step in ANSYS. The pressure on the potshell from absorption of chemicals cannot be reliably calculated, even though carbon block expansion due to sodium absorption is known. Alternatively, instead of using many assumptions in a so called "Half empty shell" or "Almost empty shell" models available as options at DUBAL, an "Empty shell" model was used [3] with imposed uniform pressure on the inside surface over the height of the cathode block, expanded by 200 mm above and 140 mm below the block, such that the measured horizontal deformation of the cell was obtained. The vertical forces applied were the weight of metal, bath, freeze and cathode lining distributed uniformly over the potshell area as well as the weight of the superstructure as point loads on the end deckplates. An adjustment factor for the true weight of new lining was used to match the measured vertical deformation of the potshell. Figure 14 shows the model deckplate deformation compared to the average measured values in five DX+ cells at a specific date. The model represents closely the reality and is considered to be validated.

CFD Models of Cell Gas Evacuation

The purpose of the CFD modeling of gas evacuation is to design the interior gas collection system so that it provides good gas evacuation for all circumstances in cell operation, such as opening the cell doors and the hoods. The CFD model is based on PHOENICS. It is fully 3-D in order to represent the opening of any hood, but for normal operation and tapping, half of the model

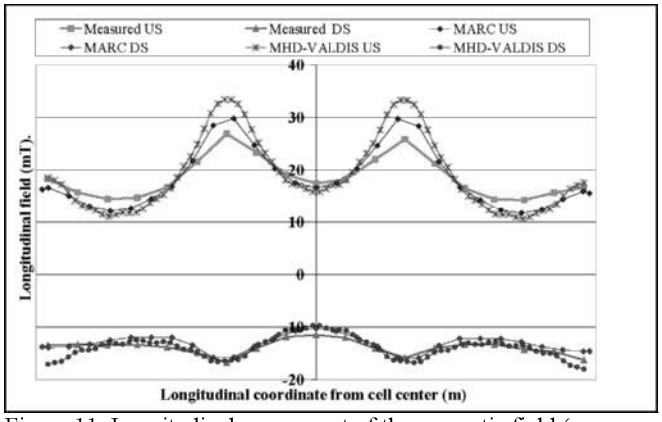

Figure 11. Longitudinal component of the magnetic field (average of three cells) above crust in DX+ cells. US = Upstream, DS = Downstream.

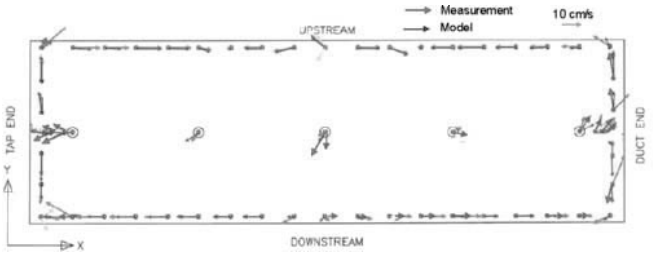

Figure 12. Validation of metal circulation model with measured velocities in DX+ cells at 420 kA.

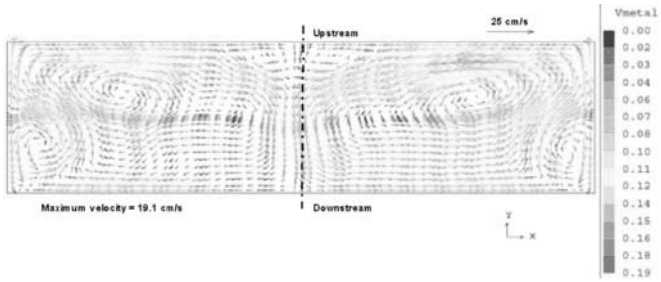

Figure 13. ESTER metal circulation patterns with calibrated velocity magnitudes in DX+ cells at 420 kA.

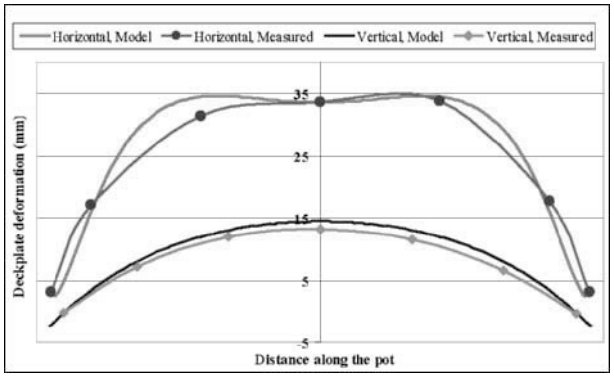

Figure 14. DX+ deckplate horizontal and vertical deformation along the pot.

with longitudinal axis symmetry is used. The model consists of gas channels inside the superstructure, under hood space with anode cover, stubs, yokes and rods, holes in the crust below the crust breakers, gaps between hoods and between rods and the superstructure and also includes some of the gas exhaust duct

outside the cell. For tapping, the doors and the tapping hole are open. For anode setting, the corresponding hoods are open.

Model input parameters are: mass flow rate in the exhaust duct, temperature of air entering the hooded space, surface temperatures of the anode cover, yokes and anode rods as well as the composition and temperature of gases emanating trough crust holes. Model outputs are pressure, temperature and velocity field. Figure 15 shows pressure distribution on a vertical plane along the cell. The 3-D model structure can also be seen. With macros, the gas mass flow rate is calculated from velocities at any specified channel cross-section. This helps validate the model. Model validation measurements were made through five holes in the superstructure which give access to the gas collection channel. Gas velocity was measured with a Pitot tube, and temperature with a sheathed thermocouple. Mass flow rate was calculated from velocities and gas density. Figure 16 shows the comparison between the model and measurements. The agreement is good. This model is considered to be validated.

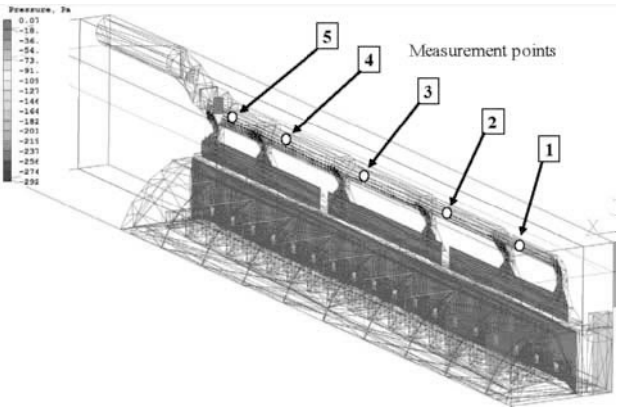

Figure 15. Pressure distribution on a vertical slice of the model.

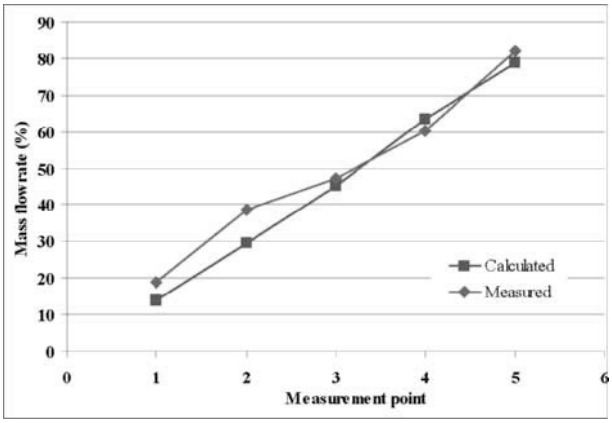

Figure 16. Calculated and measured mass flow rate in the gas collection channel (percent of total flow in exhaust duct). The measurement points are indicated with numbered white circles in Figure 15.

Conclusion

DUBAL has built and validated mathematical models of aluminium electrolysis cells. A very meticulous and thorough measurement methodology was used for model validation and experimental evaluation of the DX and DX+ cell technologies. The validity of the models has been proven and the models have already been used extensively for the design of DX+ cells and further optimisation of DX and DX+ cell technology.

Acknowledgements

Throughout the model development and measurement campaigns, there have been many people who are not mentioned in the author list, but who made valuable contributions to the success of these projects. First of all, the DUBAL measurement team showed extraordinary dedication and skill to carry out many measurement campaigns and to assure the best quality of measurements. The model development, measurement campaigns and model validation were supported by Dr. Vinko Potocnik; specific model development was supported by Dr. Marc Dupuis for ANSYS, Dr. Valdis Bojarevics for MHD-VALDIS and by CHAM for ESTER and PHOENICS models. Special thanks go to Prof. Barry Welch, for his constructive inputs on cell energy balance and process representation.

References

1. ANSYS is licenced by ANSYS Inc, 275 Technology Drive Canonsburg, PA 15317, U.S.A., http://www.ansys.com/ .
2. M. Dupuis, ANSYS-Based 3-D Thermo-Electric Heat Balance Models, Genisim Brochure, http://www.genisim.qc.ca/.
3. M. Dupuis, "Mathematical Modeling of Aluminum Reduction Cell Potshell Deformation", Light Metals (2010), 417-422.
4. PHOENICS is licenced by CHAM Ltd, Concentration, Heat and Momentum Limited, Wimbledon Village, London SW19 5AU, England, http://www.cham.co.uk/ .
5. Vinko Potocnik and Frederic Laroche, "Comparison of Measured and Calculated Metal Pad Velocities for Different Prebake Cell Designs", Light Metals (2001), 419-425.
6. Dagoberto S. Severo et al, "Comparison of Various Methods of Modeling Metal-Bath Interface Deformation", Light Metals (2008), 413-418.
7. Valdis Bojarevics, Light Metals, (2010), "Time Dependent MHD Models for Aluminium Reduction Cells", Light Metals, (2010), 199-206.
8. MARC was developed by CERCA (Centre de recherche en calcul appliqué), Montreal, Canada and is available from one of the authors (Vinko Potocnik).
9. TECPLOT is licenced by Tecplot Inc, 3535 factoria Blvd S.E., Suite 550, Bellvue, WA 98006, U.S.A., http://www.tecplot.com/.
10. Vinko Potocnik, "Measurement Techniques for Pot Analysis", *TMS 2012 Industrial Aluminum Electrolysis*, September 10 – 14, 2012, Chicoutimi, Quebec, Canada.
11. Warren Haupin, "Interpreting Cell Voltage Components", Light Metals, (1998), 531-537.
12. Hukseflux Thermal Sensors B.V., Delft, The Netherlands, http://www.hukseflux.com/.
13. Mark Taylor, "Anode Cover Material – Science, Practice and Future Needs", *Ninth Australasian Aluminium Smelter Technology Conference*, Terrigal, Australia, 4 – 9 November 2007, paper 11.
14. B.F. Bradley, E.W. Dewing, J.N. Rogers, "Metal Pad Velocity Measurements by the Iron Rod Method", Light Metals, (1984), 541-552.
15. Valdis Bojarevics and Koulis Pericleous, "Solution of the Metal-Bath Interface for Aluminium Electrolysis Cells", Light Metals, (2009), 569-574.